Journal of Materials Chemistry A

Accepted Manuscript

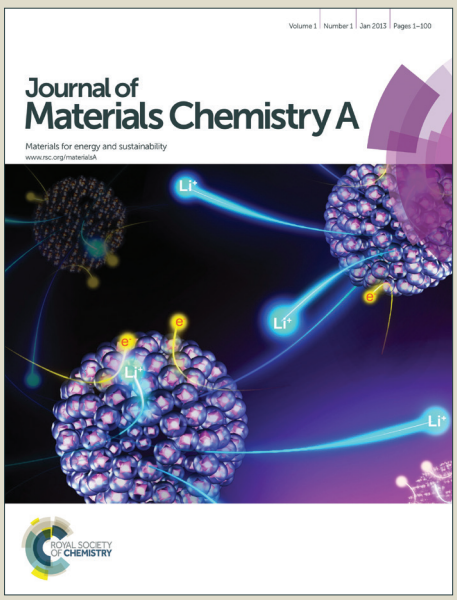

This is an *Accepted Manuscript*, which has been through the Royal Society of Chemistry peer review process and has been accepted for publication.

Accepted Manuscripts are published online shortly after acceptance, before technical editing, formatting and proof reading. Using this free service, authors can make their results available to the community, in citable form, before we publish the edited article. We will replace this *Accepted Manuscript* with the edited and formatted *Advance Article* as soon as it is available.

You can find more information about *Accepted Manuscripts* in the Information for Authors.

Please note that technical editing may introduce minor changes to the text and/or graphics, which may alter content. The journal's standard Terms & Conditions and the Ethical guidelines still apply. In no event shall the Royal Society of Chemistry be held responsible for any errors or omissions in this *Accepted Manuscript* or any consequences arising from the use of any information it contains.

ROYAL SOCIETY OF CHEMISTRY

www.rsc.org/materialsA

Journal of Materials Chemistry A RSCPublishing

ARTICLE

Enhanced Hydrogen Evolution Catalysis from Osmotic Swelled Ammoniated MoS_2†

Cite this: DOI: 10.1039/x0xx00000x

Zhuangzhi Wu,[a,b,c] Chaoyun Tang,[b] Pan zhou,[b] Zhihong Liu,[a] Yushuai Xu,[b] Dezhi Wang,*[b,c] and Baizeng Fang*[d]

Received 00th January 2015
Accepted 00th January 2015

DOI: 10.1039/x0xx00000x

www.rsc.org/

An osmotic swelled ammoniated MoS_2 electrocatalyst for hydrogen evolution is developed via a simple hydrothermal route for the first time. The applied relatively high temperature and pressure promote the diffusion of NH_4^+ ions into MoS_2 lamellar structures, leading to the formation of ammoniated MoS_2 with remarkable lattice expansion. The insertion of NH_4^+ ions induces a great enhancement in the electrical conductivity of MoS_2, resulting in an excellent activity for the hydrogen evolution reaction with a small Tafel slope of 45 mV dec^{-1}, which is amongst the best records of MoS_2-based catalysts, making it a very promising electrocatalyst to replace Pt-based ones.

1. Introduction

Due to energy crisis and environmental pollution, renewable clean energy sources are strongly demanded. Hydrogen has been vigorously pursued as one of the most promising energy carriers for the clean fuel of the future,[1-4] and has a great deal of potential applications, for examples, powering electronic devices, fuel cells, vehicles, homes and so on.[5-11] In order to generate hydrogen efficiently and environmentally friendly different strategies have been pursued.[12-15] Without natural reserves, water splitting using renewable energy in the form of electricity has been proposed as an effective way for a sustainable hydrogen evolution. The most efficient hydrogen evolution reaction (HER) catalyst is platinum (Pt). However, the low abundance and high cost prevent the massive employment of Pt for scalable hydrogen production. As a result, more earth-abundant and cheaper HER electrocatalysts have been vigorously pursued,[16,17] mainly including MoS_2,[18-20] WS_2,[21] MoC,[22,23] MoB,[23] MoP[24,25] and so on.

Among all these alternatives, nanometer-scale molybdenum disulfide (MoS_2) has received tremendous attention as a promising electrocatalyst in the HER due to its low cost, rich reserve and excellent electrocatalytic properties.[26-28] And great efforts have been made to improve the HER function over MoS_2-based electrocatalysts, including increasing the number of active sites,[27,28] enhancing the intrinsic activity of each site [29,30] and improving the electrical conductivity.[31-33] As we know, the active sites of MoS_2 for the HER are located on the edges of lamellar structures, and the basal planes are inert.[34] Therefore, on one hand, a high edge/basal ratio is required for the design of highly active MoS_2 catalysts. However, on the other hand, the intrinsic resistance is approximately 2200 times smaller along a basal plane than perpendicularly between sheets.[35] The high edge/basal ratio with high active site density also means a large resistance, hindering the enhancement of HER activity. Thus, balancing the benefits between high active site density and good conductivity becomes the most important and challenging issue for the design of highly active MoS_2 HER catalysts.

To gain the balance, Lukowski et al firstly synthesized flowerlike 2H-MoS_2 nanostructures with a high active site density, and then exfoliated them into metallic monolayer 1T-MoS_2 nanosheets, revealing an excellent HER activity with a Tafel slope of 54 mV dec^{-1} (43 mV dec^{-1} after *IR* correction).[36]

[a]*School of Metallurgy and Environment, Central South University, Changsha 410083, China.*
[b]*School of Materials Science and Engineering, Central South University, Changsha 410083, China. Tel: +86 731-88830202. Email: dzwang@csu.edu.cn (D. Wang)*
[c]*Key Laboratory of Ministry of Education for Non-ferrous Materials Science and Engineering, Central South University, Changsha 410083, China.*
[d]*Department of Chemical & Biological Engineering, University of British Columbia, 2360 East Mall, Vancouver, B.C., Canada V6T 1Z3. Email: bfang@chbe.ubc.ca (B. Fang)*

†Electronic Supplementary Information (ESI) available: XPS spectra for the annealed A-MoS_2, polarization curves and the derived Tafel plots for the A-MoS_2 catalysts obtained at different temperatures/with various mass loadings, cycling performance of the annealed A-MoS_2. See DOI: 10.1039/x0xx00000x /.

Journal of Materials Chemistry A Accepted Manuscript

However, the metallic 1T-MoS_2 is a meta-stable phase, and easy to form 2H-MoS_2 at a higher temperature (above 95 °C).[37] Xie et al proposed defect-rich MoS_2 ultrathin nanosheets prepared by a facile hydrothermal method as highly active HER catalysts, in which the active sites and conductivity can be adjusted separately by controlling the addition content of sulfurization agent and preparation temperature, respectively, showing an excellent activity with Tafel slopes of 50-55 mV dec^{-1}.[38,39] Recently, Tan et al coated monolayer MoS_2 films onto the 3D nanoporous metals to obtain extra active sites on the curved basal planes and improve the conductivity at the same time, leading to a superior HER activity with a Tafel slope of 46 mV dec^{-1}.[40] Despite of the enormous efforts, further improvements are highly desirable to achieve the balance between high active site density and good conductivity.

In this study, we proposed the osmotic swelled MoS_2 lamellar structures as HER catalysts for the first time, in which adjacent layers are filled and expanded by ammonium ions. Although ammoniated MoS_2 was prepared recently by the reaction of NH_4Cl and Li-intercalated MoS_2 (Li_xMoS_2),[41] in contrast, we obtained ammoniated MoS_2 by a facile hydrothermal route, in which ammonium ions permeate easily into the interlayers of MoS_2, driven by the high pressure and temperature in the autoclave. Benefiting from the defect-rich nanostructures and the great enhancement of the conductivity resulting from the ammonium ion intercalation, the osmotic swelled MoS_2 lamellar structures exhibit excellent HER activity with a small Tafel slope of 45 mV dec^{-1}. Different from the conventional wisdom of adopting highly conductive supports, this work introduces a novel route to reduce the resistance between the layers by the intercalation of NH_4^+ ions, and more other guest species such as Ni, Co, K, Na, conductive organics, and so on, can also be considered to be an intercalation agent. Significantly and importantly, this work provides a novel strategy to further improve the HER function by the structure design.

2. Experimental

2.1 Synthesis of osmotic swelled MoS_2 lamellar structures

Typically, 0.88 g of $(NH_4)_6Mo_7O_{24} \cdot 4H_2O$ and 0.94 g of thioacetamide (CH_3CSNH_2) were dissolved into 50 mL of ammonia with vigorous stirring to form a homogeneous solution. Then, the solution was put into a 100 ml Teflon-lined stainless steel autoclave. With a heating rate of 10 K min^{-1}, the solution was heated up to 220°C and maintained for 13 h. The whole reaction system was cooled to room temperature. Next, the final samples can be obtained after centrifugation (8000 rpm), washing (water and ethanol) and drying (333 K), and marked as A-MoS_2 (ammoniated MoS_2).

2.2 Characterizations

X-ray powder diffraction (XRD) patterns were collected using a D/max-2500 system with Cu Kα radiation (λ = 0.154 nm). Raman spectroscopy was recorded using the instrument LabRAMHR-800 of French company HRIBA. The composites were further confirmed by the X-ray photoelectron spectroscopy (XPS). The microstructures were observed by the scanning electron microscopy (SEM, FEI Sirion 200) and scanning transmission electron microscopy (STEM, JEOL2100). DSC/TGA analyses were performed with SDT.Q600 (Tainstruments, USA).

2.3 Preparation of electrodes and electrochemical characterization

3 mg of catalyst and 80 μL of Nafion solution (5 wt%) were dispersed into 1 mL of a solution composed of 4:1 (v/v) distilled water and ethanol. After sonication for 30 min, 5 μL of the mixed solution was dropped onto the surface of a GCE (glassy carbon electrode, 3 mm in diameter). Subsequently, the catalyst-coated GCE was dried at room temperature, and the obtained final HER catalyst has a loading of 213 μg cm^{-2}.

The electrochemical tests were conducted in a standard three-electrode setup at a CHI 660E electrochemical station. Linear sweep voltammetry (LSV) was performed in 0.5 M H_2SO_4 (purged with pure Ar) at room temperature with a scan rate of 2 mV s^{-1} using a saturated calomel electrode (SCE) as the reference electrode and a glassy carbon as the counter electrode. All the potentials were calibrated to a reversible hydrogen electrode (RHE).

3. Results and discussion

3.1 Characteristics of the as-synthesized catalysts

The expanded lamellar structure of A-MoS_2 was confirmed by the XRD pattern, as shown in Fig. 1a. Generally, the (002) diffraction peak of MoS_2 is located at 14.4° (JCPDS card: 65-1951), but the intercalation of ammonia species induced the splitting of typical peak of (002), leading to two separated diffraction peaks located at 9.2° and 18.4°, respectively, which can be attributed to the expansion of interlayers.[41] Moreover, calculated by the Scherrer equation, the basal spacing increases about 3.45 Å compared to the standard pristine MoS_2 (JCPDS card: 65-1951), which matches well with the size of NH_4^+ ion whose diameter is about 3.5 Å. The observed increase in the interlayer spacing here is comparable to those reported in other ammoniated layered chalcogenides.[42,43] To confirm the crystal phase, the A-MoS_2 was annealed at 400° C for 2 h to remove the inserted NH_4^+ ions. Interestingly, one can see that the obtained XRD pattern is in a good agreement with the standard pristine MoS_2 with a basal spacing of 6.2 Å, which is only slightly larger than the standard value of 6.15 Å, indicating a slight lattice expansion due to the existence of crystal defects.[44] However, it must be noted that the A-MoS_2 exhibits much better crystallinity than other counterparts prepared at the same temperature of 220 ° C without addition of ammonia,[19,38,39] which is demonstrated by much sharper reflection peaks.

Journal of Materials Chemistry A Accepted Manuscript

 This journal is © The Royal Society of Chemistry 2015

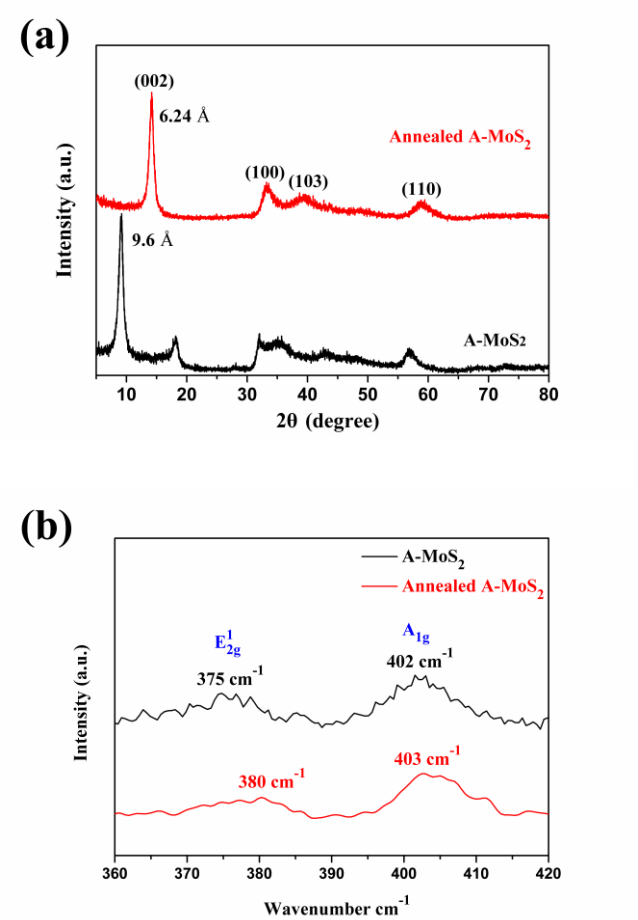

Fig. 1 Typical XRD patterns (a) and Raman spectra (b) of the as-synthesized and the annealed A-MoS_2

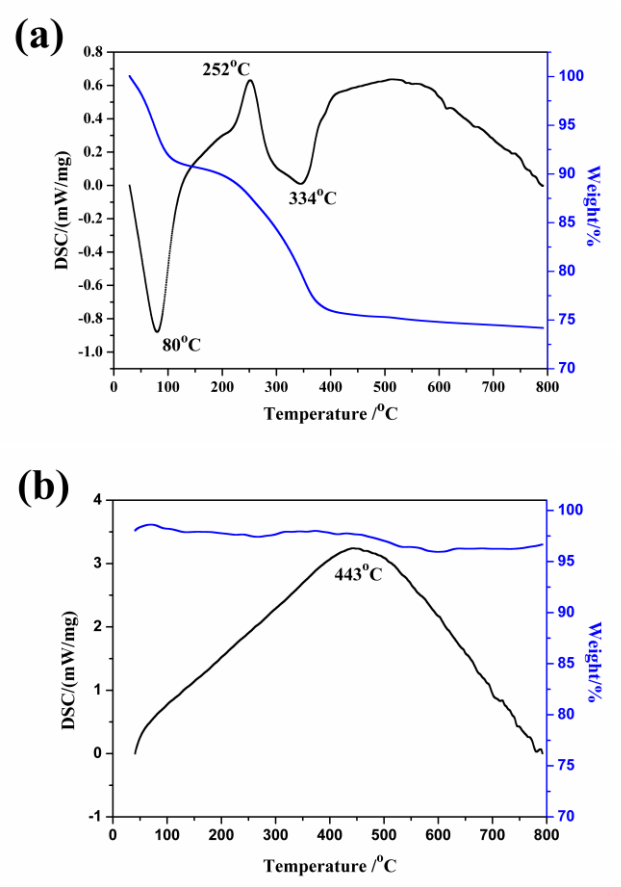

Fig. 2 DSC/TG curves of the A-MoS_2 (a) and the annealed A-MoS_2 (b).

Fig. 1b compares the Raman spectra of the as-synthesized and annealed A-MoS_2. Both of the typical E_{2g} and A_{1g} peaks of MoS_2 crystal are observed. As we know, the E_{2g} correlates with the relative vibration mode along the layer of bond between Mo and S, and presents the inlayer displacements of Mo and S atoms.[45] The broaden peak width and weaker intensity indicate the existence of crystal defects in the base planes of MoS_2.[46] Generally, when the layer number increases, the interlayer Van der Waals force in MoS_2 suppresses atom vibration, leading to higher force constants and blue-shift of A_{1g} mode.[47] However, compared to the bulk MoS_2 (408 cm^{-1}),[47] a remarkable red-shift of A_{1g} over the A-MoS_2 is observed (402 cm^{-1}), indicating a much less stacking height. After the annealing process, the stacking height is increased slightly, revealed by the blue-shift of A_{1g} to 403 cm^{-1}.

To further confirm the existence of the inserted species, DSC/TGA measurements were performed. As shown in Fig. 2a, there are two distinct mass loss steps centered at 80 and 334 °C over A-MoS_2, respectively, associated with two remarkable endothermic peaks. The first mass loss step can be attributed to the release of the inserted water, H_3O^+ and possible NH_3 (10%),[41] and the second one can only be attributed to the inserted NH_4^+ ions (16%). Obviously, in the present case, the ammoniated MoS_2 shows much better stability than the ones in previous reports,[41,48,49] in which NH_4^+ ions were released at much lower temperatures (i.e., 240 °C). Morever, there is an obvious exothermic peak at 252 °C, revealing a structure conversion to the thermodynamically stable 2H-MoS_2.[38] However, no remarkable mass loss can be observed over the annealed A-MoS_2, indicating the absence of any inserts, as shown in Fig. 2b. And there is also an exothermic peak at 443 °C caused by the structure conversion.

To provide a direct evidence, chemical composition of the as-synthesized and annealed A-MoS_2 were further analyzed by XPS. As shown in Fig. 3 and Fig. S1 (ESI), the A-MoS_2 is mainly composed of Mo, S and N elements, but the annealed A-MoS_2 only contains Mo and S elements. As evident in Fig. 3a, two characteristic peaks of Mo $3d_{3/2}$ and Mo $3d_{5/2}$ orbitals are located at 232.4 and 229.3 eV, respectively, indicating the dominance of Mo^{4+}.[38] The S 2p region (Fig. 3b) also exhibits two doublets located at 160.5 and 161.6 eV, corresponding to $2p_{3/2}$ and $2p_{1/2}$, respectively, consistent with a -2 oxidation state for the sulphur.[26,38] Moreover, the peak at 168 eV can be ascribed to the small amount of SO_4^{2-} residue,[50] which is eliminated after the annealing treatment, as shown in Fig. S1b. Most interestingly and importantly, the N 1s spectrum (Fig. 3c) located at 402.2 eV demonstrates the existence of NH_4^+,[41] indicating the successful synthesis of ammoniated MoS_2.

Journal of Materials Chemistry A Accepted Manuscript

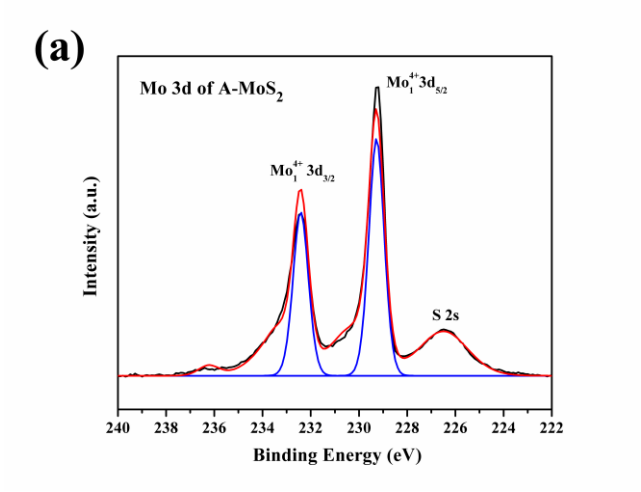

Fig. 3 XPS spectra of the A-MoS_2: (a) Mo 3d, (b) S 2p, (c) N 1s.

Moreover, the absence of N 1s over the annealed A-MoS_2 further confirms that the inserted NH_4^+ has been completely removed, as revealed in Fig. S1c. Different from the

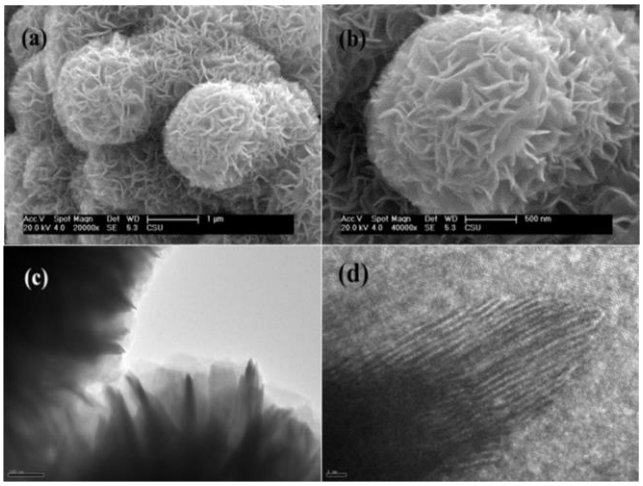

Fig. 4 SEM (a, b) and TEM (c, d) images of the A-MoS_2.

observations in Jeffery et al's report,[41] in our case, no NH_3 is observed, and thus the actual chemical composition of the as-synthesized A-MoS_2 should be defined as $(NH_4)^+_xMoS_2$, in which x is about 1.92 (calculated by the mass loss).

Fig. 4 shows the representative SEM and TEM images of the A-MoS_2. Generally, MoS_2 obtained by a hydrothermal method tends to form flakes due to its intrinsic lamellar structures, and then these flakes aggregate together to form microspheres in order to reduce surface energy.[19] We can see that the A-MoS_2 samples are microspheres assembled by nanoflakes with sizes of 1-2 μm (Fig. 1a and b). Moreover, the TEM images further confirm the spherical morphology and typical lamellar structure of 2H-MoS_2, as shown in Fig. 4c and d. However, it must be noted that the A-MoS_2 is much larger than the NH_4^+-free MoS_2 obtained by the same hydrothermal route,[19] which exhibit nanoflowers with a diameter of 100-500 nm. And the latter shows lower stacking height of lamellar structures, indicating worse crystallinity, consistent with the XRD analysis. Therefore, we can conclude that the existence of ammonia promotes the crystallinity and results in crystal growth, as revealed by the XRD pattern, SEM and TEM images.

3.2 Electrocatalytic tests

The polarization curves were measured in 0.5 M H_2SO_4 with a scan rate of 2 mV s^{-1} at room temperature and shown in Fig. 5a. As a reference, we demonstrated the HER activity of the commercial Pt/C catalyst (Johnson Matthey, 20 wt %) exhibiting high HER catalytic performance with an extraordinary low overpotential and a high current density. And it is evident that the NH_4^+-free A-MoS_2 after annealing at 400° C shows much smaller current density than the as-synthesized A-MoS_2, and only a little higher than that of the bare GC (glassy carbon) electrode, which can be attributed to less exposed active sites and larger interlayer resistance. On one hand, the annealing process at a high temperature of 400° C further promotes the crystal growth and increases the stacking height, resulting in huge particles with less available exposed

Journal of Materials Chemistry A Accepted Manuscript

 This journal is © The Royal Society of Chemistry 2015

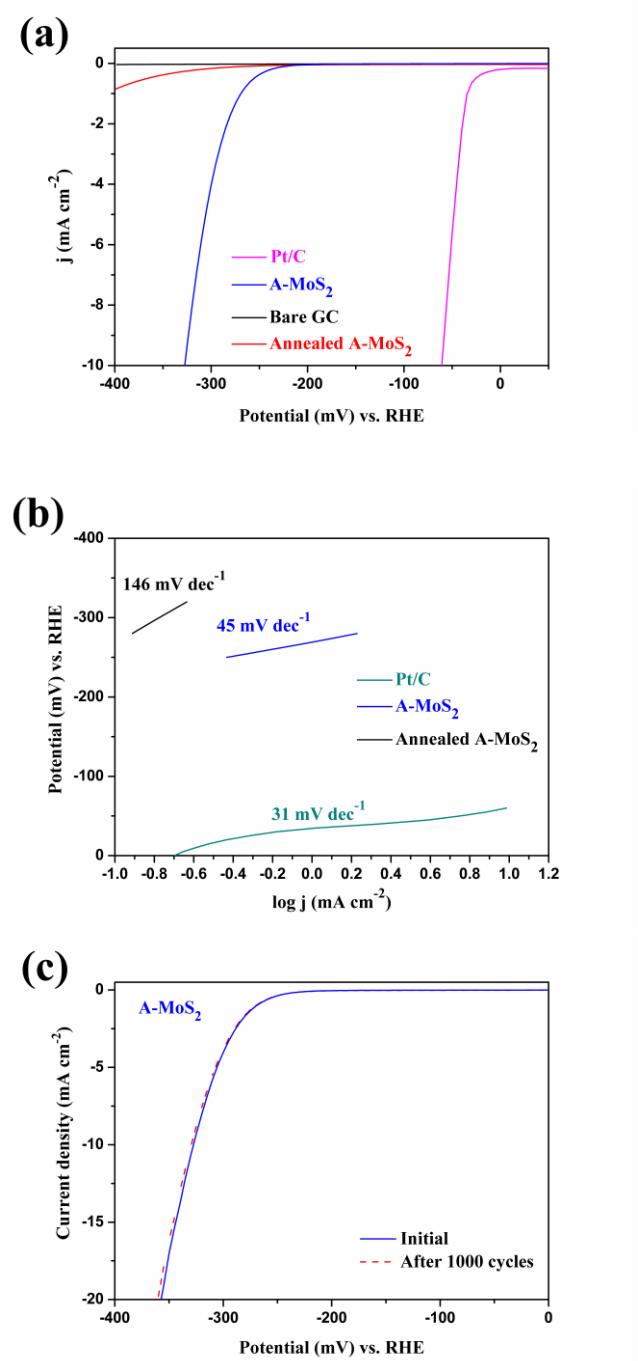

Fig. 5 Polarization curves (a), the derived Tafel plots (b) for the various catalyst electrode materials, and the durability test (c) of the as-synthesized A-MoS_2.

active sites. On the other hand, it should be noted that the resistance between layers of MoS_2 is much larger than that in layers, which will greatly deteriorate the HER activity,[50] and the resistance of the annealed A-MoS_2 will be greatly enhanced due to the increased stacking height and the release of NH_4^+ ions, which are supposed to help reduce the electric resistance between the layers. As a result, the current density of the annealed A-MoS_2 is decreased sharply.

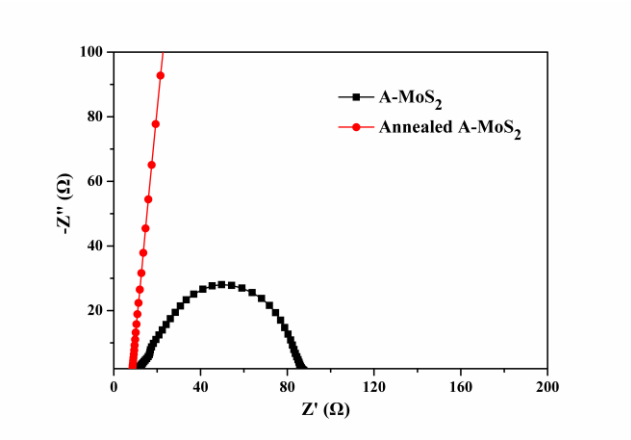

Fig.6 Nyquist plots of the various MoS_2 catalysts.

Generally, the Tafel slope represents the intrinsic activity of HER catalysts, and smaller Tafel slopes mean faster HER rates with the increased overpotentials. The Tafel slopes derived from the polarization curves are fitted to the Tafel equation (η =b log j + a, where j is the current density and b is the Tafel slope), and shown in Fig. 5b. Obviously, the A-MoS_2 exhibits a very small Tafel slope of 45 mV dec^{-1}, which is amongst the best records over the MoS_2-based HER catalysts, smaller than those of the MoS_2 nanoflowers (52 mV dec^{-1}),[19] oxygen-incorporated MoS_2 ultrathin nanosheets (55 mV dec^{-1}),[38] defect-rich MoS_2 ultrathin nanosheets (50 mV dec^{-1}),[39] which were also prepared by the hydrothermal method. After removing NH_4^+ ions by annealing at 400 ℃, the Tafel slope is increased remarkably up to 146 mV dec^{-1}, which can be attributed to the greatly enhanced resistance between the layers and less exposed active sites, coincident with the small current density in Fig. 5a. However, it is still smaller than that of bulk MoS_2 microparticles (186 mV dec^{-1}).[19] Furthermore, the observed Tafel slope of 45 mV dec^{-1} in this work suggests that the HER takes place via a rapid Volmer reaction followed by a rate-limiting Heyrovsky step and the Volmer-Heyrovsky mechanism is operative in the HER catalyzed by the ammoniated MoS_2, according to the classical theory for HER in acidic media.[51]

To investigate the influences of preparation temperature and mass loading on the HER performances, the polarization curves and the derived Tafel plots were also shown in Fig. S2 and Fig. S3. One can see that the mass loading of 3 mg results in the smallest Tafel slope of 45 mV dec^{-1}. With the increase of preparation temperature, the current density is also enlarged gradually and reaches the maximum at 220°C, and then turns down at higher temperature of 240°C, which is similar to the trend of MoS_2 nanoflowers.[19] Accordingly, the Tafel slope also follows the similar trend, in which the Tafel slopes of A-MoS_2 obtained at low temperatures (160-200°C) are reduced gradually with the increase of preparation temperature and achieve the minmum value at 220 °C, and then turns up at 240 °C. And the largest value of 77 mV dec^{-1} is obtained at 160 °C, indicating the worst HER function, consistent with the smallest current density in Fig. S2b. With the increased mass loading,

Journal of Materials Chemistry A Accepted Manuscript

the specific current density of A-MoS_2 is increased gradually, and the corresponding Tafel slope is reduced accordingly, reaching the minimum value of 45 mV dec^{-1} with a mass loading of 3 mg, and then turns up, as revealed in Fig. S3.

Durability is another significant criterion to evaluate a catalyst. To probe the durability of the A-MoS_2 catalyst in an acidic environment, polarization measurements of the A-MoS_2 were carried out continuously in 0.5 M H_2SO_4. After 1000 cycles, there is only slight decay in the current density, indicating a good durability, consistent with that reported for other MoS_2-based catalysts.[19,38,39] Moreover, the durability of annealed A-MoS_2 was also evaluated, demonstrating the similar stability (Fig. S4).

To get a better understanding of the improvement mechanism of the A-MoS_2, electrochemical impedance spectroscopy (EIS) measurements were also performed. Fig. 6 shows the representative Nyquist plots of the EIS response at 320 mV for the GCEs modified by different catalysts, including the A-MoS_2 and annealed A-MoS_2. It is clear that the A-MoS_2 exhibits one capacitive semicircle, indicating that the corresponding equivalent circuit for the HER was characterized by one time constant and the reaction is kinetically controlled. Moreover, the diameter of semicircle for the A-MoS_2 is very small, indicating a smaller charge transfer resistance about 88 Ω, which can be attributed to the insertion of NH_4^+ ions, enhancing the electrical conductivity. However, after being annealed at 400 ^oC, the charge transfer resistance of the A-MoS_2 is greatly increased due to the release of conductive NH_4^+ ions. Furthermore, the annealing process also promotes the crystal growth of MoS_2, resulting in higher stacking. As we know, the intrinsic resistance of MoS_2 between layers is very large,[35] and the increased stacking height means much larger resistance. Therefore, it can be concluded that both of the release of NH_4^+ ions and the increased stacking height contribute to the extremely large resistance of the annealed A-MoS_2, leading to much worse HER activity (Fig. 5).

4. Conclusions

In summary, the osmotic swelled ammoniated MoS_2 has been successfully developed via a simple hydrothermal route and adopted as a HER catalyst for the first time, exhibiting excellent activity with a small Tafel slope of 45 mV dec^{-1}, which is amongst the best records reported for the MoS_2-based HER catalysts, making it a very promising HER catalyst to replace Pt-based catalysts. The insertion of NH_4^+ ions into MoS_2 lamellar structures induces a great improvement of electrical conductivity, resulting in better HER performance. This work introduces a new method to prepare ammoniated transition metal dichalcogenides and a novel strategy to further improve the HER function by the structure design.

Acknowledgements

Financial supports from the National Natural Science Foundation of China (Grant No. 51302326), the Postdoctoral Science Foundation of China (Grant No. 2013M531801) and Yu-Ying Program of Central South University are gratefully acknowledged.

Notes and references

1 H. Vrubel and X. Hu, *ACS. Catal.*, 2013, **3**, 2002−2011.
2 A. B. Lausen, S. Kegnas, S. Dahl and I. Chorkendorff, *Energy. Environ. Sci.*, 2012, **5**, 5577−5591.
3 D. Xu, Q. Chu,Z. Wu, Q. Chen, S. Fan, G. Yang and B. Fang, *J. Catal.* 2015, **325**, 118−127.
4 B. Fang, J. Kim, M. Kim and J. Yu, *Acc. Chem. Res.*, 2013, **46**, 397−1406.
5 B. Fang, J. Kim, M. Kim and J. Yu, *Chem. Mater.*, 2009, **21**, 789–796.
6 B. Fang, N. Chaudhari, M. Kim, J. Kim and J. Yu, *J. Am. Chem. Soc.*, 2009, **131**, 15330–15338.
7 Y. Wang, N. Zhou, B. Fang, H. Li, X. Bi and H. Wang, *Chem. Rev*. in press, DOI: 10.1021/cr500519c.
8 B. Fang, S. Iwasa, Y. Wei, T. Arai, M. Kumagai, *Electrochim. Acta.*, 2002, **47**, 3971−3976.
9 J. Kim, B. Fang, M. Kim, V. Tricoli and J. Yu, *Catal. Today.*, 2009, **146**, 25–30.
10 M. Kim, B. Fang, N. Chaudhari, M. Song, T. Bae and J. Yu, *Electrochim. Acta.*, 2010, **55**, 4543–4550.
11 C. Tang, D. Wang, Z. Wu and B. Duan, *Int. J. Hydrogen. Energy.*, 2015, **40**, 3229-3237.
12 Y. Xing, B. Fang, A. Bonakdarpour, S. Zhang, D. Wilkinson, *Int. J. Hydrogen Energy.*, 2014, **39**, 7859–7867.
13 B. Fang, H. Zhou, I. Honma, *J. Phys. Chem. B.*, 2006, **110**, 4875−4880.
14 Y. Wang, G. Chang, Q. Chen, G. Yang, S. Fan and B. Fang, *Chem. Commun.*, 2015, **51**, 685−688.
15 S. Yang, G. Chang, G. Yang, Y. Wang and B. Fang, *Catal. Sci. Technol*., 2015, **5**, 228−233.
16 P. Xiao, Y. Yan, X. Ge, Z. Liu, J. Wang and X. Wang, *Appl. Catal. B: Environ.*, 2014, **154-155**, 232−237.
17 H. Du, S. Gu, R. Liu, C. M. Li, *J. Power Sources.*, 2015, **278**, 540−545.
18 D. Wang, Z. Wang, C. Wang, P. Zhou, Z. Wu and Z. Liu, *Electrochem. Commun.*, 2013, **34**, 219−222.
19 D. Wang, P. Zhou, Z. Wu, Z. Wang and Z. Liu, *J. Power Sources.*, 2014, **264**, 229−234.
20 Y. Yan, B. Xia, N. Li, Z. Xu, A. Fisher and X. Wang, *J. Mater. Chem. A.*, 2015, **3**, 131-135.
21 Z. Wu, B. Fang, A. Bonakdarpour, A. Sun, D. P. Wilkinson and D. Wang, *Appl. Catal. B: Environ.*, 2012, **125**, 59−66.
22 W. Chen, C. Wang, K. Sasaki, N. Marinkovic, W. Xu, J. T. Muckerman, Y. Zhu and R. Adzic, *Energy Environ. Sci.*, 2013, **6**, 943−951.
23 H. Vrubel and X. Hu, *Angew. Chem. Int. Ed.*, 2012, **51**, 12703−12706.
24 X. Chen, D. Wang, Z. Wang, P. Zhou, Z. Wu and F. Jiang, *Chem. Commun.*, 2014, **50**, 11683−11685.
25 Z. Xing, Q. Liu, A. Asiri and X. Sun, *Adv. Mater.*, 2014, **26**, 5702−5707.
26 J. Kibsgaard, Z. Chen, B. N. Reinecke and T. F. Jaramillo, *Nature. Mater.*, 2012, **11**, 963−969.

Journal of Materials Chemistry A Accepted Manuscript

 This journal is © The Royal Society of Chemistry 2015

27 D. Kong, H. Wang, J. J. Cha, M. Pasta, K. J. Koski, J. Yao and Y. Cui, *Nano. Lett.*, 2013, **13**, 1341−1347.
28 Z. Wu, B. Fang, Z. Wang, C. Wang, C. Wang, Z. Liu, F. Liu, W. Wang, A. Alfantazi, D. Wang and D. P. Wilkinson, *ACS. Catal.*, 2013, **3**, 2101−2107.
29 D. Merki, H. Vrubel, L. Rovelli, S. Fierro and X. Hu, *Chem. Sci*., 2012, **3**, 2515−2525.
30 J. Bonde, P. G. Moses, T. F. Jaramillo, J. K. Norskov and I. Chorkendorff, *Faraday. Discussions.*, 2008, **140**, 219−231.
31 Y. Li, H. Wang, L. Xie, Y. Liang, G. Hong and H. Dai, *J. Am. Chem. Soc.*, 2011,**133**, 7296−7299.
32 X. Ge, L. Chen, L. Zhang, Y. Wen, A. Hirata and M. Chen, *Adv. Mater*., 2014, **26**, 3100−3104.
33 T. Wang, J. Zhuo, K. Du, B. Chen, Z. Zhu, Y. Shao and M. Li, *Adv. Mater*., 2014, **26**, 3761−3766.
34 T. F. Jaramillo, K. P. Jorgensen, J. Bonde, J. H. Nielsen, S. Horch and I. Chorkendorff, *Science*, 2007, **317**, 100−102.
35 J. D. Benck, T. R. Hellsterm, J. Kibsgaard, P. Chakthranont and T. F. Jaramillo, *ACS. Catal*., 2014, **4**, 3957−3971.
36 M. A. Lukowski, A. S. Daniel, F. Meng, A. Forticaux, L. Li, S. Jin, *J. Am. Chem. Soc.*, 2013, **135**, 10274−10277.
37 F. Wypych and R. Schollhorn, *J. Chem. Soc., Chem. Commun.*,1992, **19**, 1386−1388.
38 J. Xie, J. Zhang, S. Li, F. Grote, X. Zhang, H. Zhang, R. Wang, Y. Lei, B. Pan and Y. Xie, *J. Am. Chem. Soc.*,2013, **135**, 17881−17888.
39 J. Xie, H. Zhang, S. Li, R. Wang, X. Sun, M. Zhou, J. Zhou, X. Wen and Y. Xie, *Adv. Mater*.,2013, **25**, 5807−5813.
40 Y. Tan, P. Liu, L. Chen, W. Cong, Y. Ito, J. Han, X. Guo, Z. Tang, T. Fujita, A. Hirata and M. Chen, *Adv. Mater*., 2014, **26**, 8023−8028.
41 A. A. Jeffery, C. Nethravathi and M. Rajamathi, *J. Phys. Chem. C.*, 2014, **118**, 1386−1396.
42 F. R. Gamble, J. H. Osiecki, M. Cais, R. Pisharody, F. J. Disalvo and T. H. Geballe, *Science.*, 1971, **174**, 493−497.
43 R. Schollhorn and A. Weiss, *J. Less. Commun. Metals.*, 1974, **36**, 229−236.
44 Z. Wu, D. Wang and A. Sun, *J. Cryst. Growth.*, 2010, **312**, 340−343.
45 C. Lee, H. Yan, L. E. Brus, T. F. Heinz, J. Hone and S. Ryu, *ACS Nano.*, 2010, **4**, 2695−2700.
46 K. Liu, W. Zhang, Y. Lee, Y. Lin, M. Chang, C. Su, C. Chang, H. Li, Y. Shi, H. Zhang, C. Lai and L. Li, *Nano. Lett.*, 2012, **12**, 1538−1544.
47 H. Li, Q. Zhang, C. C. R. Yap, B. K. Tay, T. H. T. Edwin, A. Olivier and D. Baillargeat, *Adv. Fun. Mater*., 2012, **22**, 1385−1390.
48 M. J. Mckelvy and W. S. Glaunsinger, *J. Solid. State. Chem.*, 1987, **67**, 142−150.
49 E. W. Ong and J. Eckert, *Chem. Mater*., 1994, **6**, 1946−1954.
50 Y. Yan, B. Xia, X. Qi, H. Wang, R. Xu, J. Wang, H. Zhang and X. Wang, *Chem. Commun*.,2013, **49**, 4884−4886.
51 B. E. Conway and B. V. Tilak, *Electrochim. Acta*., 2002, **47**, 3571−3594.

Journal of Materials Chemistry A Accepted Manuscript

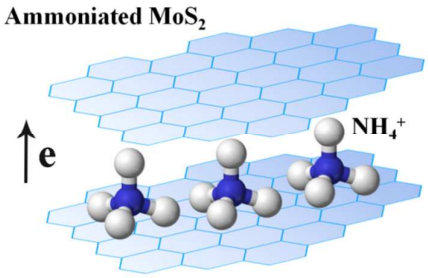

Osmotic swelled ammoniated MoS_2 was obtained via a facile hydrothermal route, exhibiting excellent HER performances due to improved electric conductivity.

Journal of Materials Chemistry A Accepted Manuscript